



Published in final edited form as:

Magn Reson Med. 2012 December ; 68(6): 1866–1875. doi:10.1002/mrm.24210.

Free-Breathing Cardiac MR with a Fixed Navigator Efficiency Using Adaptive Gating Window Size

Mehdi H. Moghari¹, Raymond H. Chan¹, Susie N. Hong-Zohlman¹, Jaime L. Shaw¹, Lois A. Goepfert¹, Kraig V. Kissinger¹, Beth Goddu¹, Mark E. Josephson¹, Warren J. Manning^{1,2}, and Reza Nezafat¹

¹Department of Medicine (Cardiovascular Division), Harvard Medical School and Beth Israel Deaconess Medical Center, Boston, MA

²Department of Radiology, Harvard Medical School and Beth Israel Deaconess Medical Center, Boston, MA

Abstract

A respiratory navigator with a fixed acceptance gating window is commonly used to reduce respiratory motion artifacts in cardiac MR. This approach prolongs the scan time and occasionally yields an incomplete dataset due to respiratory drifts. To address this issue, we propose an adaptive gating window approach in which the size and position of the gating window are changed adaptively during the acquisition based on the individual's breathing pattern. The adaptive gating window tracks the breathing pattern of the subject throughout the scan and adapts the size and position of the gating window such that the gating efficiency is always fixed at a constant value. To investigate the image quality and acquisition time, free breathing cardiac MRI, including both targeted coronary MRI and late gadolinium enhancement (LGE) imaging, was performed in 67 subjects using the proposed navigator technique. Targeted coronary MRI was acquired from eleven healthy adult subjects using both the conventional and proposed adaptive gating window techniques. Fifty-six patients referred for cardiac MRI were also imaged using LGE with the proposed adaptive gating window technique. Subjective and objective image assessments were used to evaluate the proposed method. The results demonstrate that the proposed technique allows free-breathing cardiac MRI in a relatively fixed time without compromising imaging quality due to respiratory motion artifacts.

Keywords

Free-breathing cardiovascular MRI; respiratory motion compensation; diaphragmatic navigators; gating window

INTRODUCTION

The development of diaphragmatic navigators and bellows gating (1–6) has resulted in free-breathing three-dimensional (3D) cardiovascular magnetic resonance imaging (MRI) with minimal respiratory motion artifacts. The linear relationship between the respiratory motion of the right hemi-diaphragm (RHD) and the heart (7) allows diaphragmatic navigators to track the RHD motion to indirectly correct the respiratory motion of the heart. During a preparation phase, the RHD position is measured to determine its location at end-expiration; a small gating window, typically 5–7 mm, is placed around the end-expiratory position.

Immediately before each acquisition of k-space lines, the RHD position is measured. If the RHD position is within the gating window, the acquired k-space lines are accepted for image reconstruction. Otherwise, those lines are rejected and reacquired until they are all acquired within the gating window. This procedure, the so-called accept/reject algorithm (2,4,8), may be used with or without a slice tracking factor to acquire images with sub-millimeter accuracy (9,10). The diaphragmatic navigator successfully suppresses the respiratory motion of the heart along the superior-inferior (SI) direction, but this approach prolongs the scan due to the need to reacquire the rejected k-space lines and results in an unpredictable scan acquisition time (11–13).

There have been several attempts to improve the gating efficiency and reduce the scan acquisition time without compromising image quality using k-space weighting (14,15), phase encode reordering (16–18), and diminishing variance algorithms (19). These algorithms reduce the acquisition time, but changes in breathing pattern, and therefore the distribution of RHD positions throughout the scan, can strongly reduce gating efficiency. To mitigate this problem and maintain a high gating efficiency, an end-expiratory following technique has also been proposed to track the position of the RHD at end-expiration and update the location of the gating window (20,21). Although there is no image degradation using this technique compared to the fixed gating window position, the scan time and the range of diaphragm positions in the final image are still unpredictable and can be prolonged (22,23).

Phase ordering with Automatic Window Selection (PAWS) and Continuously Adaptive Window Averaging (CLAWS) have been also proposed as alternative methods to the accept/reject algorithm to appropriately account for drifts and variations in breathing patterns (22,24). In these approaches, it is assumed that the data acquired at any RHD position maybe used to reconstruct the final image. Therefore, k-space lines are accepted and reordered using a predetermined algorithm to avoid duplications at different RHD positions. The scan is completed when all k-space lines are acquired within a gating window around an RHD position. These algorithms efficiently complete scans within a gating window in the presence of drifts and variations in breathing pattern, but their scan acquisition times are still long and unpredictable (23).

In this study, we propose an alternative respiratory navigator for free-breathing cardiac MR, in which the size and position of the gating window of the navigator is adaptively determined for each subject based on a subject-specific breathing pattern to maintain a constant gating efficiency throughout a scan.

MATERIALS AND METHODS

Adaptive Gating Window Algorithm

A diaphragmatic navigator is placed at the dome of the RHD to track the position. The first N positions are used for the preparation phase, in which the center and the size of gating window are determined. The acquired RHD positions are used to generate a respiratory profile of the breathing pattern, as shown in Figure 1A. Multiple bins with a size of 0.5 mm are used to produce a histogram of the breathing pattern and the total number of the RHD positions in the histogram, i.e. N , is 50.

As shown, the upper side of gating window, Y , is placed at the maximum RHD location, representing end-expiration. The lower side of gating window, X , is placed where $\alpha\%$ of the RHD locations in the histogram are within the gating window, i.e. gating efficiency is $\alpha\%$. The gating efficiency, α , is determined by the operator as a user input. Since the respiratory profile is generated from discrete 0.5 mm bins, there might not be a position for X where the

gating efficiency is exactly $\alpha\%$. In that case, the first position where the gating efficiency is greater than $\alpha\%$ is chosen for X .

During the imaging phase, an RHD location will be measured before each acquisition of k -space lines. If the RHD location is within the gating window (with a size of $Y-X$), the acquired k -space lines are accepted for image reconstruction; otherwise the lines are rejected and reacquired in the next cardiac cycle. Meanwhile, the newly measured RHD position is added to the respiratory profile and the oldest point in the respiratory profile is removed from the profile to maintain the number of RHD positions in the respiratory profile at a constant value of $N=50$. Based on the newly added RHD location, the probability distribution of RHD positions and upper and lower sides of the gating window are updated for the next k -space lines acquisitions such that the gating efficiency is always equal or greater than $\alpha\%$. Figure 1B shows an example of the variation of the size of gating window throughout the scan to maintain a constant gating efficiency, $\alpha = 40\%$. Figure 1C demonstrates the trace of the RHD motion measured by the RHD navigator and the size and position of the gating window defined by the proposed algorithm. As shown, the gating window size has been adaptively modified to keep the gating efficiency constant. In Figures 1B and 1C, the first 20 k -space segments are acquired in the preparation phase and not used in reconstruction.

The proposed adaptive gating window technique can automatically decrease the size of the gating window in subjects with regular breathing patterns who have a high gating efficiency to better gate the respiratory motion and minimize respiratory motion artifacts. Additionally, in subjects with irregular breathing patterns and low gating efficiency, where scans are long and could potentially fail due to drifts, the proposed algorithm automatically increases the gating window size to maintain a constant gating efficiency of $\alpha\%$ and complete the scan. In this case, the mean size of gating window might be wider than the standard 5–7 mm; therefore, image quality may be compromised but the scan can be completed in a given time.

Imaging Studies

The proposed adaptive gating window technique was implemented on a whole-body 1.5T MRI scanner (Achieva, Philips Healthcare, Best, the Netherlands) with a 5-channel phased coil array. Before imaging, written informed consent was obtained and imaging protocols were approved by our IRB.

Imaging in Healthy Subjects

To investigate the efficacy of the proposed method for different pre-determined fixed gating efficiencies in comparison to the conventional fixed gating window size, coronary MRI was performed in 11 healthy adult subjects (8 female, age 27 ± 14 years). A targeted right coronary artery (RCA) sequence was used to image the RCA using the conventional diaphragmatic navigator technique with the standard 5 mm gating window size, as previously described (25). Briefly, scout images were first acquired to localize the anatomy using a balanced steady-state free precession (SSFP) sequence with 3.1×3.1 mm² in-plane resolution and 10 mm slice thickness. From these, a diaphragmatic 2D pencil beam navigator was placed at the dome of the RHD. An axial breath-hold cine image with a resolution of 2.0×2.0 mm² and slice thickness of 8 mm was acquired using an SSFP cine sequence to visually identify the RCA diastolic period. A low resolution 3D coronary survey (resolution of $2.0 \times 2.0 \times 4.0$ mm³) was acquired during the rest period of the RCA using an ECG-triggered SSFP sequence and the diaphragmatic navigator with 8 mm gating window. The low resolution 3D coronary survey images were used to define the imaging plane of RCA using a 3-point method (25). A free-breathing 3D ECG-triggered SSFP sequence with the following parameters: field of view (FOV) = $290 \times 290 \times 45$ mm³; spatial resolution =

$1.0 \times 1.0 \times 3.0 \text{ mm}^3$ reconstructed to a resolution of $0.57 \times 0.57 \times 1.5 \text{ mm}^3$; TE/TR = 2.9/5.8 ms; flip angle = 110° ; 20 k-space lines in a segment acquired at every cardiac cycle (TFE factor) and no parallel imaging methods were used. The scan time was 4 minutes and 48 seconds assuming a heart rate of 65 beats per minute and 100% navigator efficiency. Four other RCA images were also acquired using the same sequence parameters with the proposed adaptive gating window technique and fixed gating efficiency of 25%, 50%, 75%, and 100%.

Patient Study

To assess the impact of the proposed strategy on late gadolinium enhancement (LGE) MRI (26), we studied 56 patients referred for clinical CMR including 29 patients (12 female, 60 ± 10 years) with atrial fibrillation referred for pre (n=19) or post (n=10) pulmonary vein (PV) isolation and 27 patients (10 female, 48 ± 13 years) referred for the assessment of left ventricular scar/fibrosis. All subjects received a bolus infusion of 0.2 mmol/kg of Gd-DTPA (Magnevist, Bayer Schering Pharma AG, Germany). In the patient study, only the proposed adaptive gating window algorithm was used for imaging.

Imaging Protocols

Left Atrium and Left Ventricular LGE—Fifteen to twenty minutes after contrast injection, a Look-Locker sequence (27) with a resolution of $2.7 \times 2.7 \times 10 \text{ mm}^3$ was used to determine the appropriate inversion time such that the left ventricular myocardium signal was nulled. A 3D LA LGE dataset was then acquired using an inversion recovery gradient echo sequence with a diaphragmatic navigator with the proposed adaptive gating window technique with a fixed gating efficiency of 40–50% and the following sequence parameters: ECG-triggered at end diastole; FOV = $320 \times 400 \times 80 \text{ mm}^3$; spatial resolution = $1.4 \times 1.4 \times 4.0 \text{ mm}^3$ reconstructed to a resolution of $0.62 \times 0.62 \times 2.0 \text{ mm}^3$ using zero padding; TE/TR = 2.5/5.2 ms; flip angle = 25° ; TFE factor = 22. No parallel imaging techniques were used and the scan acquisition time was 4 minutes and 52 seconds for a heart rate of 60 beats per minutes assuming 100% navigator efficiency. Twenty-four patients were imaged with a constant gating efficiency of 40%, and five were imaged with 50% gating efficiency.

Similar to the 3D LA LGE and with the same imaging parameters, a 3D LV LGE dataset was acquired using a diaphragmatic navigator with the proposed adaptive gating window technique with a fixed gating efficiency of 40–50%. Thirteen patients were imaged with a constant gating efficiency of 40% and 6 patients were imaged with a constant gating efficiency of 50%.

A few patients (n = 8, 2 female, 51 ± 8 years) were also imaged using a 3D free-breathing phase-sensitive inversion recovery (PSIR) sequence (28) with the following imaging parameters: FOV = $320 \times 320 \times 90 \text{ mm}^3$; spatial resolution = $1.8 \times 2.0 \times 10.0 \text{ mm}^3$ reconstructed to a resolution of $1.25 \times 1.25 \times 5.0 \text{ mm}^3$ using zero padding; TE/TR = 2.3/4.8 ms; flip angle = 15° ; TFE factor = 25. No parallel imaging methods were used. The scan time was 1 minute and 12 seconds for a heart rate of 65 beats per minute assuming 100% gating efficiency. In PSIR acquisition 4 patients were imaged with 40% gating efficiency and 4 were imaged with 50% gating efficiency.

Image and statistical Analysis

All images were reconstructed online using the MR console. Raw navigator data, which includes the position of the RHD throughout a scan, was saved from the scanner to report the actual gating efficiency in scans acquired using the proposed adaptive gating window technique. In the patient study where the proposed adaptive gating window technique was only used for imaging, the navigator data was recorded and used to calculate the projected

gating efficiency if the 5 mm gating window technique had been used in the image acquisition. To calculate the projected gating efficiency, the navigator data from a preparation phase was used to determine the end-expiration and the center of gating window. A 5 mm gating window was placed around the end-expiration position to sort the RHD positions acquired within and outside the gating window. The ratio between the number of RHD positions acquired within the gating window over the total number of RHD positions through the scan was defined as the projected gating efficiency for 5 mm gating window.

The Soap Bubble tool (29) was used to quantitatively evaluate the definition of the RCA. RCA sharpness scores were calculated for both sides of the whole RCA, and the final sharpness was defined as the average score of both sides divided by the lumen signal. Qualitative assessment of the RCA images was performed by two experienced independent blinded readers with three years' experience (Level 3 CMR training) in consensus using a 4-point scale previously described in (30): 1, indicating poor or uninterpretable (coronary artery visible, with markedly blurred borders or edges); 2, fair (coronary artery visible, with moderately blurred borders or edges); 3, acceptable (coronary artery visible, with mildly blurred borders or edges); and 4, excellent (coronary artery visible, with sharply defined borders or edges). For each image, separate scores were given for the proximal, middle, and distal segments of the RCA and a segment based analysis was performed. The LGE images were also qualitatively evaluated by two blinded readers with three years' experience (Level 3 CMR training) in consensus using raw images without any reformatting. The artifacts due to respiratory motion were evaluated using a 4-point scale (1 = severe, 2 = moderate, 3 = mild, 4 = none). The readers also reported whether the images were diagnostic or not.

All data are presented as mean \pm one standard deviation. A Wilcoxon Signed-Rank test and a paired two-tailed Student's t-test as well as an F-test were performed on the qualitative and quantitative measures, where appropriate. The F-test was used as a statistical test to assess the variance or standard deviation of two data sets. A p -value of 0.05 was considered statistically significant. All the statistical analyses were performed using SAS software (V9.3, SAS Institute Inc., Cary NC).

RESULTS

Figure 2 displays four consecutive slices of the RCA images reconstructed using a diaphragmatic navigator with a constant 5 mm gating window (efficiency 68%) and the proposed adaptive gating window with 25%, 50%, 75%, and 100% constant gating efficiencies. The images acquired with the constant gating efficiency of 25% depict better vessel delineation. The vessel sharpness decreases as the gating efficiency increases. The calculated size of the gating window for the scans with 25%, 50%, 75%, and 100% gating efficiencies acquired from this subject were 2.9 ± 0.4 mm, 4.0 ± 0.3 mm, 5.4 ± 0.3 mm, and 11.2 ± 1.5 mm, respectively.

Table 1 displays the scan efficiency of the RCA images, acquired from 11 subjects, using 5 mm gating window diaphragmatic navigator and the proposed adaptive gating window with fixed 25%, 50%, 75%, and 100% gating efficiencies. The variation of scan efficiency acquired using the adaptive gating window with a fixed gating efficiency was significantly smaller from those acquired with 5 mm gating window. This verified that the scan acquisition time using the adaptive gating window was more predictable than conventional fixed 5 mm gating window.

Table 2 shows the subjective visual scores and the vessel sharpness of the RCA images from the 11 subjects that were acquired with a diaphragmatic navigator using a 5 mm gating

window and the proposed adaptive gating window with 25%, 50%, 75%, and 100% fixed gating efficiencies. By increasing the gating efficiency from 25% to 100%, the vessel sharpness and visual scoring decrease and the mean gating window size increases. The proximal, middle, and distal regions of the RCA received the highest subjective score and vessel sharpness in the images acquired using the proposed adaptive gating window with 25% gating efficiency. The scores for the proximal and distal regions of the RCA as well as the overall vessel sharpness were significantly higher than for images acquired with 5 mm gating window. The visual scoring and sharpness were not significantly different from the images acquired with 50% gating efficiency and 5 mm gating window. For the images acquired with 75% gating efficiency, the vessel sharpness drops but was not significant from the 5 mm gating window. However, the middle and distal regions of the RCA received significantly lower scores compared with 5 mm gating window. With the acquisition with 100% gating efficiency, a majority of images (7/11 proximal, 3/11 mid, and 10/11 distal) were scored 1, therefore, a reliable sharpness could have not been measured. All the segments of the RCA images scored significantly lower than the images acquired with 5 mm gating window.

Figures 3, 4, and 5 illustrate representative slices of left atrium (LA) LGE, left ventricular (LV) LGE, and PSIR images acquired from three different patients using the proposed adaptive gating window with 40% gating efficiency. The gating window size for these acquisitions was 7.8 ± 1.0 mm, 4.3 ± 0.8 mm, and 2.6 ± 0.3 mm, respectively. The images are all diagnostic with visible enhancements due to pulmonary vein ablations for atrial fibrillation (Figure 3), inflamed pericardium due to pericarditis (Figure 4), and myocardial fibrosis due to hypertrophic cardiomyopathy (Figure 5); and no evident of respiratory motion artifacts can be observed. In Figure 3, the gating window size was adaptively increased to 9 mm due to a possible drift near the end of the scan to complete the scan in a predictable time.

Figure 6 displays a slice of the 3D free-breathing PSIR long axis image acquired from a patient with suspected ischemic cardiomyopathy using the proposed adaptive gating window with 40% gating efficiency. The breathing pattern and variation of the size of gating window throughout the scan are shown in Figure 1. The gating window size during the acquisition was 6.5 ± 1.4 .

Table 3 displays the subjective scores of the LA LGE, LV LGE, and LV PSIR images acquired using the proposed adaptive gating window with a fixed gating efficiency of 40% or 50%. In LA LGE images, the scan efficiency of images acquired from 29 patients was $47 \pm 8\%$ that was significantly different from $37 \pm 21\%$, the projected scan efficiency using a 5 mm gating window. The size of gating window was 6.2 ± 3.0 mm. All images were reported as diagnostic with a respiratory artifact score of 3.4 ± 0.7 .

The scan efficiency of the images acquired from 19 patients in the LV LGE images was $48 \pm 8\%$, which was similar to the projected scan efficiency acquired with 5 mm gating window, $47 \pm 14\%$. The size of gating window was 6.0 ± 3.1 mm. Seventy percent (13 out of 19) of images were reported as diagnostic. The respiratory artifact score was 2.7 ± 0.9 .

In the LV PSIR images acquired from 8 patients, the scan efficiency was $48 \pm 7\%$ compared to the projected efficiency $37 \pm 13\%$ for 5 mm gating window. All the images were reported as diagnostic with a respiratory artifact score of 3.1 ± 0.8 .

DISCUSSION

In this study a new adaptive gating window technique for navigators was developed and assessed for free-breathing cardiac MRI. The respiratory motion pattern was used to define

the position and the size of gating window to have a relatively constant gating efficiency throughout a scan. During a scan, the proposed algorithm follows the changes in the breathing pattern and updates the position and the size of the gating window to maintain the gating efficiency at a constant value, therefore completing the scan with a fixed efficiency and predictable time.

In subjects who have regular breathing patterns and have a high gating efficiency within a 5 mm gating window, the proposed technique adaptively reduces the size of gating window to maintain a constant gating efficiency. The scan will be finished in a more predictable time frame and produce sharper images. The proposed technique also makes it possible to acquire images with a smaller gating window size, which might not be practical when using a traditional gating window with a fixed size.

The mean efficiency of scans acquired using the proposed adaptive gating window with 25% fixed gating efficiency was around 35%. This is due to the discrete 0.5 mm bin size used to generate a histogram of the breathing pattern. By decreasing the bin size to make it more continuous, the actual scan efficiency would be closer to the nominal gating efficiency defined by the operator.

In subjects with irregular breathing patterns, scans using a 5 mm gating window can take a long time and may not be completed due to drifts. In those cases, the proposed method efficiently increases the size of gating window to maintain a constant gating efficiency, therefore finishing the scan in a predictable time. Increasing the gating window size may slightly compromise the quality of images; however, the proposed technique has the advantage of completing the scan and generating images.

The proposed adaptive gating window technique completes scans in a predictable time by adaptively changing the size of the gating window throughout the scans to keep the gating efficiency constant. This procedure may lead to a gating window which is greater than the standard 5 mm size, but it has the advantage of a fixed scan time. In contrast, the diminishing variance algorithm (DVA) (19) determines the location of the RHD where the histogram is maximized and places the gating window with a fixed size of 5 mm around this position (mode). However, if the mode of the histogram varies due to a drift in the respiratory motion, the DVA algorithm becomes less efficient and the scan time increases unpredictably. On the other hand, to address the issue of variation in breathing pattern, PAWS (24) and CLAWS (22) split the respiratory cycle into even multiple 5 mm bins and assume that the data acquired at each bin might be used for the final image reconstruction. Throughout the scan, the bin in which the most data is acquired is chosen for the final image reconstruction. Although this procedure successfully addresses the problem of drifts and variations in breathing pattern and acquires the data within a fixed gating window size, the scan acquisition time is still unpredictable.

In the performed RCA study, it was shown that the quality and score of images acquired with 5 mm gating window and adaptive gating window with constant 50% gating efficiency were statistically equivalent. Therefore, in the patient study, the scan was performed with an adaptive gating window with a constant 40%- 50% gating efficiency.

The studies performed on healthy volunteers and patients using different cardiac MR sequences verified that the variation of scan acquisition time using the adaptive gating window is significantly smaller from the one acquired with a fixed gating window size of 5 mm. All images were diagnostic with negligible respiratory motion artifacts except for the 3D LGE LV sequence. In that sequence, images acquired from 6 out of 19 patients were not diagnostic mainly due to low signal to noise ratio or inaccurate inversion time (31). In (31), LGE images were acquired from 36 patients using the conventional navigator technique

with a 5 mm gating window. Sixteen LGE images were excluded due to low image quality and non-diagnostic quality caused by inaccurate inversion time and excessive blurring and ghosting artifacts. Similarly, in our study, LGE images from 6 subjects were excluded due to using an inaccurate inversion time (4 cases) and blurring and ghosting artifacts (2 cases).

In the proposed adaptive gating window technique, the last 50 positions of the right hemidiaphragm (RHD) were used to generate the histogram of the breathing pattern. The size of histogram window was kept constant by adding the newly measured location and removing the oldest location of the RHD in the histogram. This addition and removal of the RHD locations would modify the shape of the histogram and the position of the gating window. The speed of modification depends on the size of histogram window. By decreasing the size of the histogram window, the proposed adaptive gating window more quickly tracks the changes in the breathing pattern and there would be a smaller time delay in tracking the changes in the breathing pattern using the proposed adaptive gating window algorithm.

We have used the histogram size of 50 creating the upper bound delay of 50 times the period of cardiac cycle, which is less than a minute for a heart rate greater than 50 beats per minute. The optimum size of histogram window is not yet known and requires further investigation.

In our study, we did not use slice tracking. Commonly, a fixed factor of 0.6 is used for slice tracking in high-resolution cardiac MR. For a smaller gating window mismatch between the “true” tracking factor and fixed 0.6 results in insignificant residual respiratory motion; however, for larger gating windows (>7 mm) the residual motion may become significant. With the proposed technique the gating window size could be increased greater than the conventional 5 mm window in the presence of respiratory drift, hence slice tracking was not used. Although slice tracking could be integrated with the proposed technique with the availability of subject-specific tracking factor (32,33), this was not studied and requires further investigation.

The presented study has several limitations. A side by side comparison between the proposed and conventional gating window techniques in a subject with drifts in breathing pattern was not possible due to difficulties in recruiting a subject whose breathing pattern drifts twice in two separate imaging scans.

A direct comparison of the images acquired using the proposed technique and a fixed gating window size of 5 mm was not possible in patients due to the increased scan time and contrast washout effect associated with serial scan acquisition. Only the proposed adaptive gating window strategy was used for gating the respiratory motion of the heart. The impact of the proposed technique in gating and tracking the respiratory-induced heart motion should also be investigated. The order of coronary MRI scans in the healthy subjects was not randomized. Therefore, there might be changes in the breathing pattern over time, which is not accounted for. We did not use the proposed adaptive gating window for imaging of the coronary arteries in patients with coronary artery disease due to difficulty in patient recruitment and a large number of patients needed. In our study, respiratory drifts mainly occurred toward the end of the scan. There was no case where the drift occurred at the beginning of the scan. Future work should be performed to assure the diagnostic quality of the images acquired using the proposed technique in these cases.

CONCLUSION

A fixed efficiency adaptive gating window strategy is proposed and evaluated for compensating the respiratory motion of the heart with a predictable scan acquisition time for cardiac MRI.

Acknowledgments

The project described was supported by NIH R01EB008743-01A2. Mehdi H. Moghari acknowledges fellowship support from NSERC (Natural Sciences and Engineering Research Council of Canada).

References

1. Ehman RL, Felmlee JP. Adaptive technique for high-definition MR imaging of moving structures. *Radiology*. 1989; 173(1):255–263. [PubMed: 2781017]
2. Sachs TS, Meyer CH, Hu BS, Kohli J, Nishimura DG, Macovski A. Real-time motion detection in spiral MRI using navigators. *Magn Reson Med*. 1994; 32(5):639–645. [PubMed: 7808265]
3. Wang Y, Christy PS, Korosec FR, Alley MT, Grist TM, Polzin JA, Mistretta CA. Coronary MRI with a respiratory feedback monitor: the 2D imaging case. *Magn Reson Med*. 1995; 33(1):116–121. [PubMed: 7891525]
4. Wang Y, Rossman PJ, Grimm RC, Riederer SJ, Ehman RL. Navigator-echo-based real-time respiratory gating and triggering for reduction of respiration effects in three-dimensional coronary MR angiography. *Radiology*. 1996; 198(1):55–60. [PubMed: 8539406]
5. Danias PG, McConnell MV, Khasgiwala VC, Chuang ML, Edelman RR, Manning WJ. Prospective navigator correction of image position for coronary MR angiography. *Radiology*. 1997; 203(3):733–736. [PubMed: 9169696]
6. McConnell MV, Khasgiwala VC, Savord BJ, Chen MH, Chuang ML, Edelman RR, Manning WJ. Comparison of respiratory suppression methods and navigator locations for MR coronary angiography. *AJR Am J Roentgenol*. 1997; 168(5):1369–1375. [PubMed: 9129447]
7. Wang Y, Riederer SJ, Ehman RL. Respiratory motion of the heart: kinematics and the implications for the spatial resolution in coronary imaging. *Magn Reson Med*. 1995; 33(5):713–719. [PubMed: 7596276]
8. Oshinski JN, Hofland L, Mukundan S Jr, Dixon WT, Parks WJ, Pettigrew RI. Two-dimensional coronary MR angiography without breath holding. *Radiology*. 1996; 201(3):737–743. [PubMed: 8939224]
9. McConnell MV, Khasgiwala VC, Savord BJ, Chen MH, Chuang ML, Edelman RR, Manning WJ. Prospective adaptive navigator correction for breath-hold MR coronary angiography. *Magn Reson Med*. 1997; 37(1):148–152. [PubMed: 8978644]
10. Stuber M, Botnar RM, Danias PG, Kissinger KV, Manning WJ. Submillimeter three-dimensional coronary MR angiography with real-time navigator correction: comparison of navigator locations. *Radiology*. 1999; 212(2):579–587. [PubMed: 10429721]
11. McLeish K, Hill DL, Atkinson D, Blackall JM, Razavi R. A study of the motion and deformation of the heart due to respiration. *IEEE T Med Imaging*. 2002; 21(9):1142–1150.
12. Sakuma H, Ichikawa Y, Chino S, Hirano T, Makino K, Takeda K. Detection of coronary artery stenosis with whole-heart coronary magnetic resonance angiography. *J Am Coll Cardiol*. 2006; 48(10):1946–1950. [PubMed: 17112982]
13. Kato S, Kitagawa K, Ishida N, Ishida M, Nagata M, Ichikawa Y, Katahira K, Matsumoto Y, Seo K, Ochiai R, Kobayashi Y, Sakuma H. Assessment of coronary artery disease using magnetic resonance coronary angiography: a national multicenter trial. *J Am Coll Cardiol*. 2010; 56(12):983–991. [PubMed: 20828652]
14. Weiger M, Bornert P, Proksa R, Schaffter T, Haase A. Motion-adapted gating based on k-space weighting for reduction of respiratory motion artifacts. *Magn Reson Med*. 1997; 38(2):322–333. [PubMed: 9256114]
15. Sinkus R, Bornert P. Motion pattern adapted real-time respiratory gating. *Magn Reson Med*. 1999; 41(1):148–155. [PubMed: 10025623]
16. Jhooti P, Wiesmann F, Taylor AM, Gatehouse PD, Yang GZ, Keegan J, Pennell DJ, Firmin DN. Hybrid ordered phase encoding (HOPE): an improved approach for respiratory artifact reduction. *J Magn Reson Imaging*. 1998; 8(4):968–980. [PubMed: 9702900]

17. Jhooti P, Keegan J, Gatehouse PD, Collins S, Rowe A, Taylor AM, Firmin DN. 3D coronary artery imaging with phase reordering for improved scan efficiency. *Magn Reson Med*. 1999; 41(3):555–562. [PubMed: 10204880]
18. Huber ME, Hengesbach D, Botnar RM, Kissinger KV, Boesiger P, Manning WJ, Stuber M. Motion artifact reduction and vessel enhancement for free-breathing navigator-gated coronary MRA using 3D k-space reordering. *Magn Reson Med*. 2001; 45(4):645–652. [PubMed: 11283993]
19. Sachs TS, Meyer CH, Irarrazabal P, Hu BS, Nishimura DG, Macovski A. The diminishing variance algorithm for real-time reduction of motion artifacts in MRI. *Magn Reson Med*. 1995; 34(3):412–422. [PubMed: 7500881]
20. Deshpande, VS.; Krishnam, MS.; Ruehm, SG.; Finn, JP.; GA, L. Noncontrast MR angiography of the heart and great vessels using SSFP with non-selective excitation. Proceedings of the 14th scientific meeting of the International Society for Magnetic Resonance in Medicine; Seattle, WA. 2006. p. 383
21. Krishnam MS, Tomasian A, Deshpande V, Tran L, Laub G, Finn JP, Ruehm SG. Noncontrast 3D steady-state free-precession magnetic resonance angiography of the whole chest using nonselective radiofrequency excitation over a large field of view: comparison with single-phase 3D contrast-enhanced magnetic resonance angiography. *Invest Radiol*. 2008; 43(6):411–420. [PubMed: 18496046]
22. Jhooti P, Keegan J, Firmin DN. A fully automatic and highly efficient navigator gating technique for high-resolution free-breathing acquisitions: Continuously adaptive windowing strategy. *Magn Reson Med*. 2010; 64(4):1015–1026. [PubMed: 20593372]
23. Jhooti P, Haas T, Kawel N, Bremerich J, Keegan J, Scheffler K. Use of respiratory biofeedback and CLAWS for increased navigator efficiency for imaging the thoracic aorta. *Magn Reson Med*. 2011; 66(6):1666–1673. [PubMed: 21523822]
24. Jhooti P, Gatehouse PD, Keegan J, Bunce NH, Taylor AM, Firmin DN. Phase ordering with automatic window selection (PAWS): a novel motion-resistant technique for 3D coronary imaging. *Magn Reson Med*. 2000; 43(3):470–480. [PubMed: 10725891]
25. Stuber M, Botnar RM, Danias PG, Sodickson DK, Kissinger KV, Van Cauteren M, De Becker J, Manning WJ. Double-oblique free-breathing high resolution three-dimensional coronary magnetic resonance angiography. *J Am Coll Cardiol*. 1999; 34(2):524–531. [PubMed: 10440168]
26. Kim RJ, Wu E, Rafael A, Chen EL, Parker MA, Simonetti O, Klocke FJ, Bonow RO, Judd RM. The use of contrast-enhanced magnetic resonance imaging to identify reversible myocardial dysfunction. *N Engl J Med*. 2000; 343(20):1445–1453. [PubMed: 11078769]
27. Look DC, Locker DR. Time saving in measurement of NMR and EPR relaxation times. *Rev Sci Instrum*. 1972; 41(2):250–252.
28. Kellman P, Arai AE, McVeigh ER, Aletras AH. Phase-sensitive inversion recovery for detecting myocardial infarction using gadolinium-delayed hyperenhancement. *Magn Reson Med*. 2002; 47(2):372–383. [PubMed: 11810682]
29. Etienne A, Botnar RM, Van Muiswinkel AM, Boesiger P, Manning WJ, Stuber M. “Soap-Bubble” visualization and quantitative analysis of 3D coronary magnetic resonance angiograms. *Magn Reson Med*. 2002; 48(4):658–666. [PubMed: 12353283]
30. Kim WY, Danias PG, Stuber M, Flamm SD, Plein S, Nagel E, Langerak SE, Weber OM, Pedersen EM, Schmidt M, Botnar RM, Manning WJ. Coronary magnetic resonance angiography for the detection of coronary stenoses. *N Engl J Med*. 2001; 345(26):1863–1869.
31. Peters DC, Appelbaum EA, Nezafat R, Dokhan B, Han Y, Kissinger KV, Goddu B, Manning WJ. Left ventricular infarct size, peri-infarct zone, and papillary scar measurements: A comparison of high-resolution 3D and conventional 2D late gadolinium enhancement cardiac MR. *J Magn Reson Imaging*. 2009; 30(4):794–800. [PubMed: 19787731]
32. Henningson, M.; Arancibia, S.; Wiethoff, A.; Batchelor, P.; Botnar, R. Real-time adaptive motion correction for coronary MR angiography. Proc 17th Int Soc Magn Reson Med-ISMRM; Honolulu, Hawaii. 2009. p. 4645
33. Moghari MH, Hu P, Kissinger KV, Goddu B, Goepfert L, Ngo L, Manning WJ, Nezafat R. Subject-specific estimation of respiratory navigator tracking factor for free-breathing cardiovascular MR. *Magn Reson Med*. 2011 (in press).

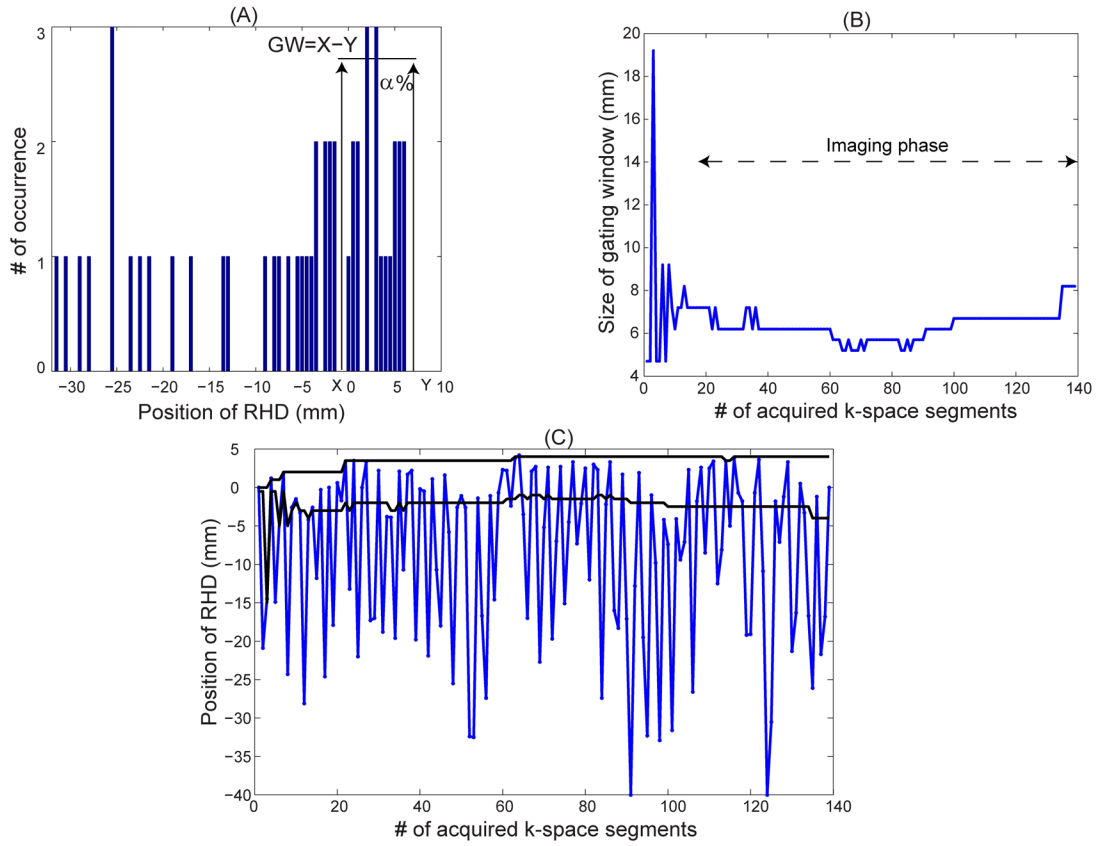


Figure 1. A) A sample histogram of the first 50 positions of the right hemi-diaphragm (RHD) in a subject and adaptively defined gating window (GW) for a gating efficiency of $\alpha = 40\%$. The histogram bin size is 0.5 mm. X and Y are the upper and lower sides of the gating window. B) An example of gating window variation over time acquired from a subject to keep the gating efficiency constant at $\alpha = 40\%$ throughout a scan. C) Trace of the RHD position (blue line), and acceptance window (black line) calculated adaptively using the proposed technique.

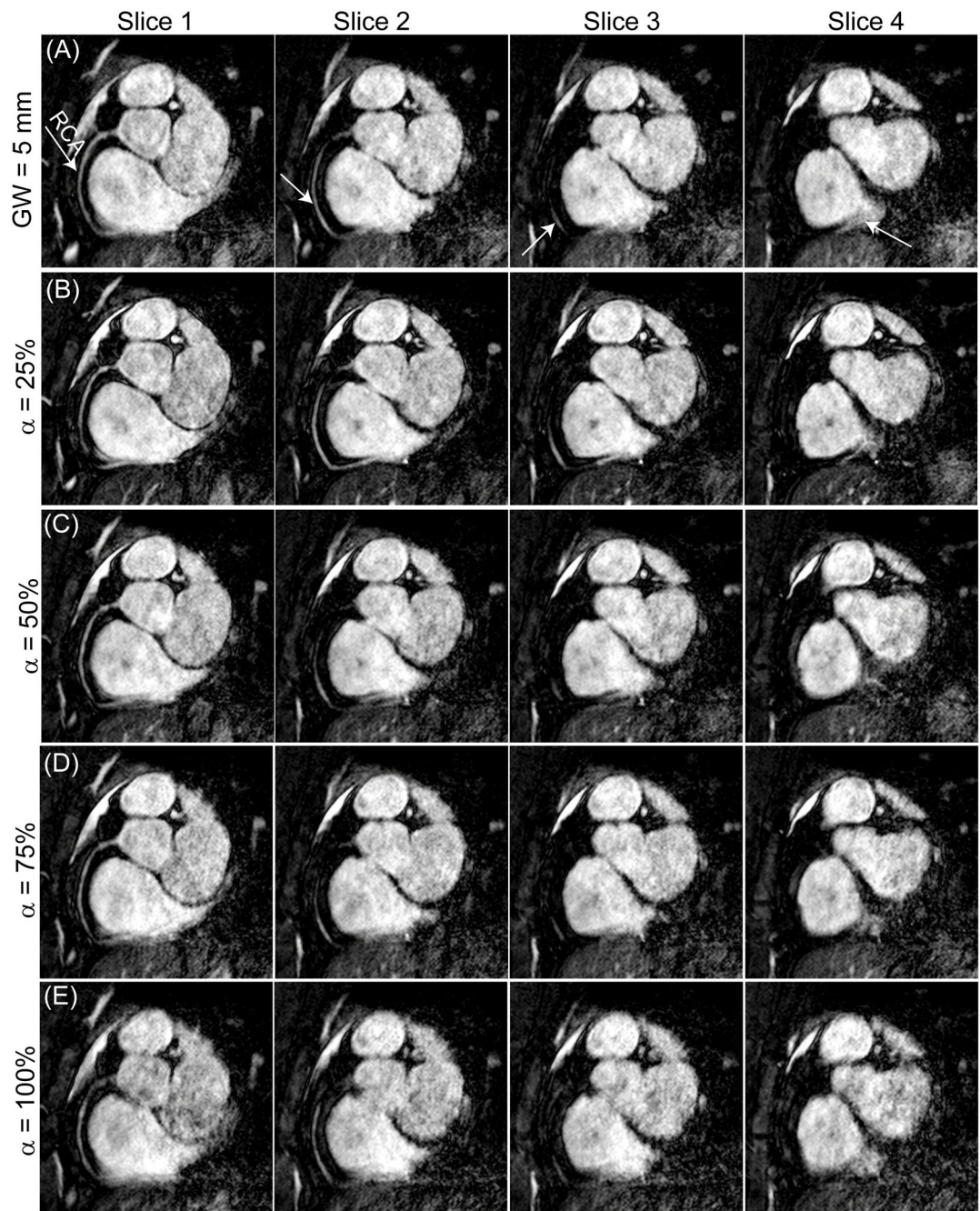


Figure 2. Four slices of the right coronary artery (RCA) acquired using a diaphragmatic navigator with (A) a fixed gating window (GW) of 5 mm (efficiency = 68%); (B–E) adaptive gating window with a fixed gating efficiency of 25%, 50%, 75% and 100%.

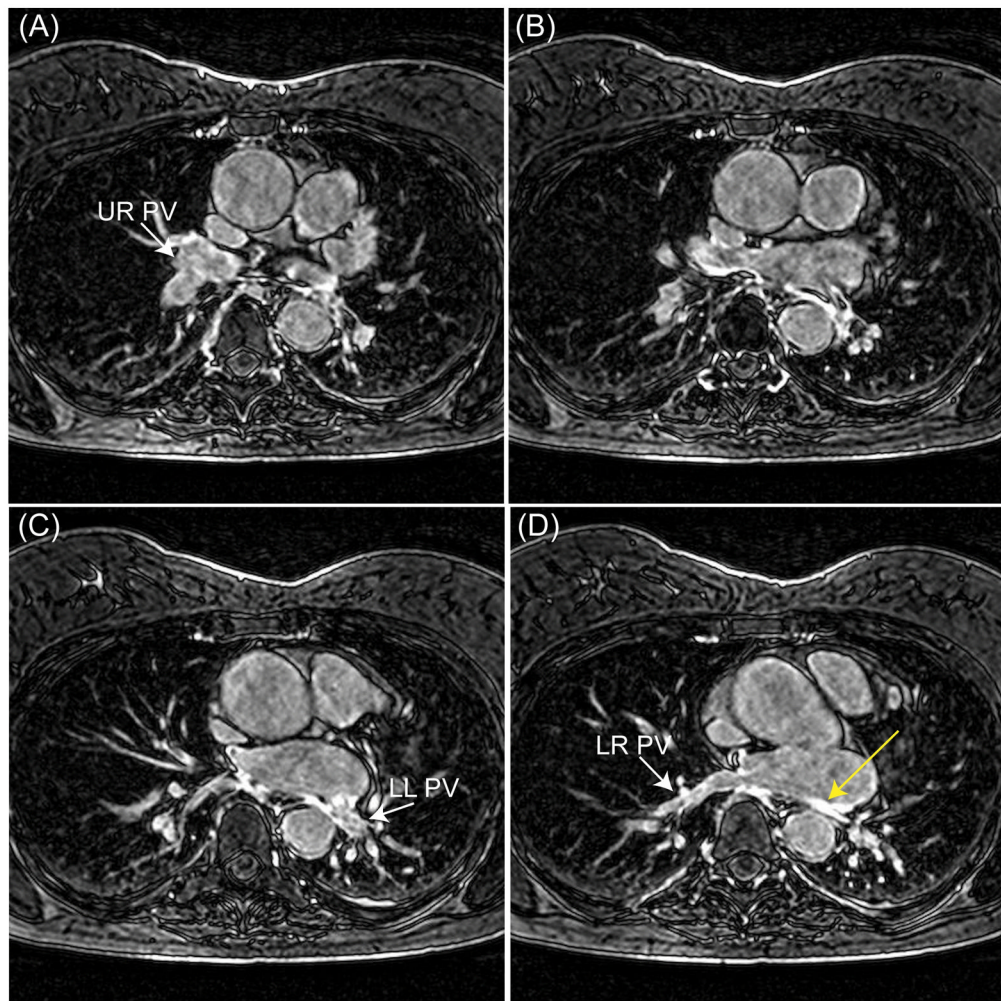


Figure 3. Four slices of a pulmonary vein (PV) and left atrium (LA) late gadolinium enhancement (LGE) image acquired from a patient after PV isolation using an adaptive gating window with a fixed gating efficiency of 40%. The mean size of gating window for this acquisition was 7.8 mm. The white arrows in the figures (A), (C), and (D), respectively, show the upper right (UR) PV, lower left (LR) PV, and lower right (LR) PV. The yellow arrow demonstrates an enhancement due to ablations.

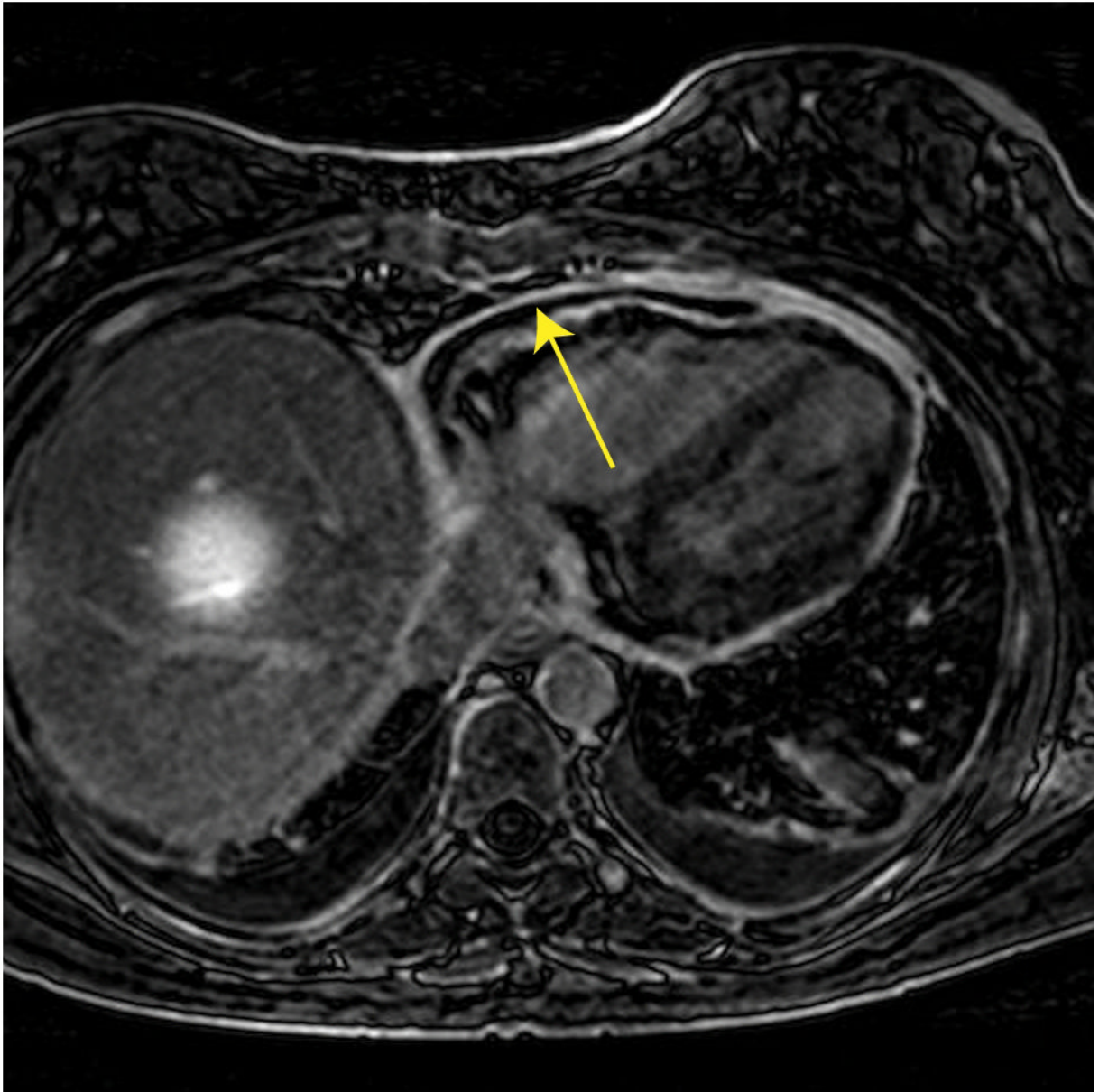


Figure 4.

A slice of a left ventricular late gadolinium enhancement (LGE) image acquired from a patient with suspected pericarditis disease using an adaptive gating window with a fixed gating efficiency of 40%. The mean size of gating window for this acquisition was 4.3 mm. The arrow demonstrates pericardial enhancement.

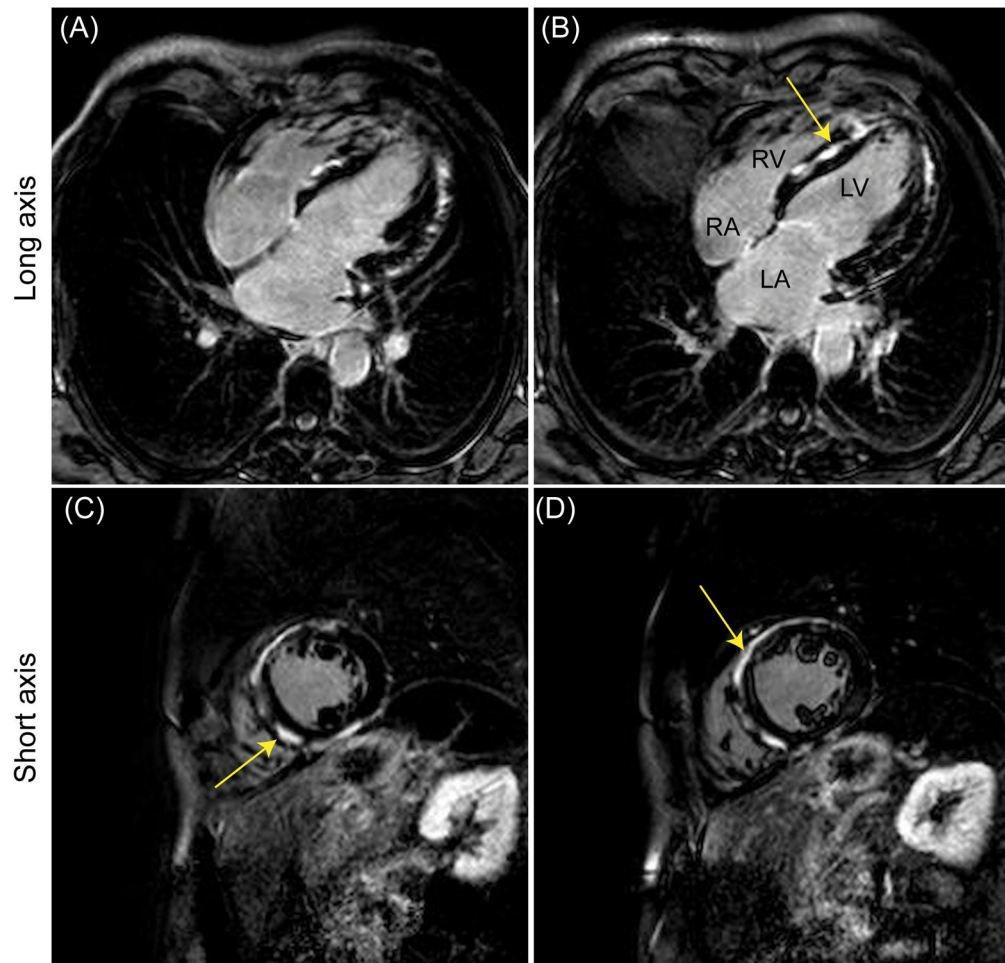


Figure 5.

Late gadolinium enhancement (LGE) long (A–B) and short (C–D) axis images acquired using a phase-sensitive inversion recovery (PSIR) sequence in a patient with suspected hypertrophic cardiomyopathy. An adaptive gating window with a user-defined efficiency of 40% was used for data acquisition resulting in an average navigator gating window of 2.6 mm. There were extensive, contiguous areas of focal hyper-enhancement (arrows) in the basal to mid antero- and infero septum, the basal to mid anterior and inferior segment, as well as the entire distal and apical walls.

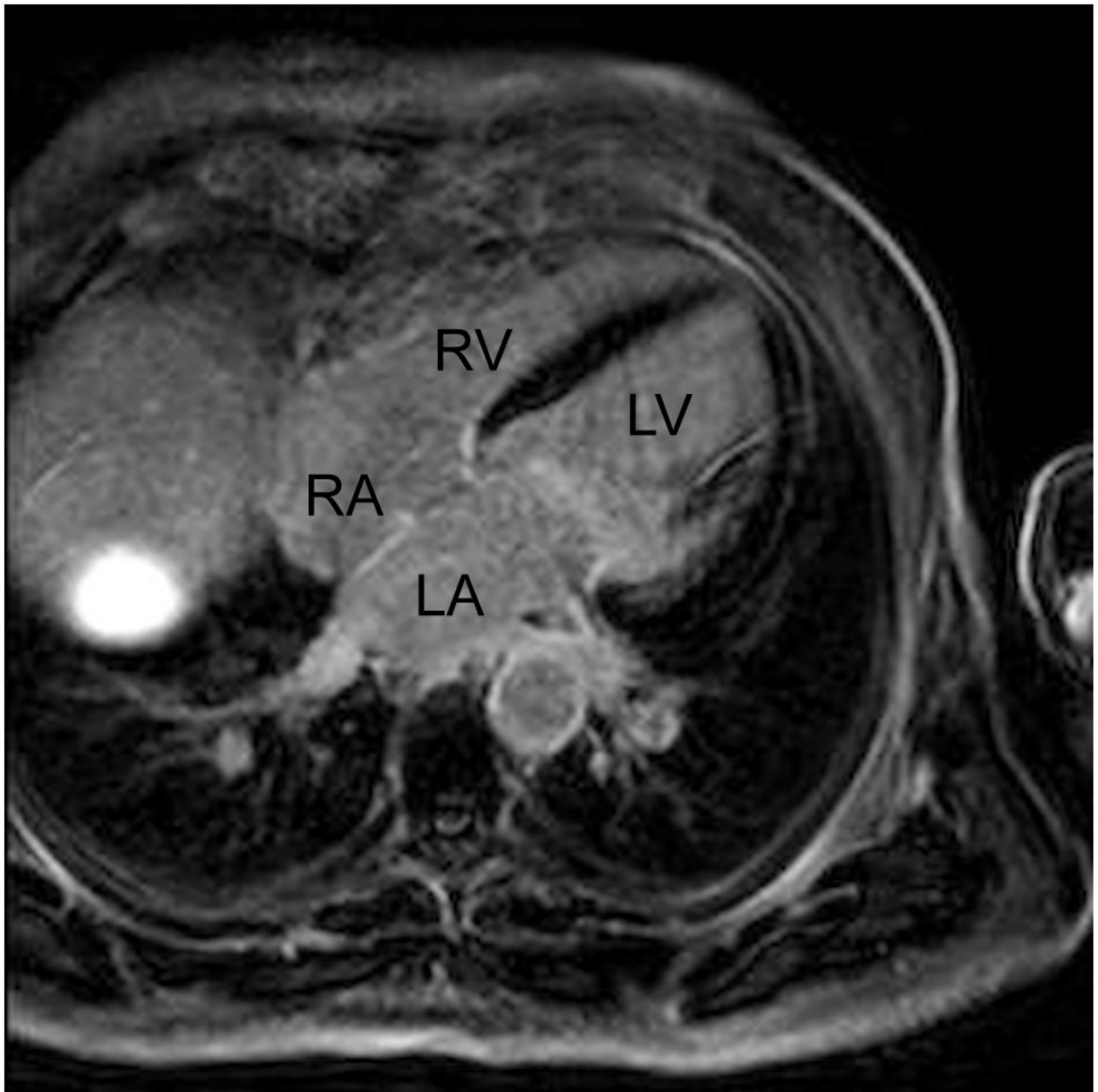


Figure 6. Representative late gadolinium enhancement (LGE) long axis image acquired using a phase-sensitive inversion recovery (PSIR) sequence from a patient with suspected ischemic cardiomyopathy. An adaptive gating window with 40% gating efficiency was used to acquire images resulting in a variable gating window size throughout the scan with an average gating window of 6.5 mm.

Table 1

Mean \pm standard deviation (std) of the gating window size and the actual scan efficiency of the targeted right coronary artery (RCA) images acquired from 11 subjects using a diaphragmatic navigator with 5 mm gating window (GW) and adaptive gating window with a fixed gating efficiency of 25%, 50%, 75%, and 100%, respectively. The statistically significant p -values comparing the scan efficiency and the variation of scan efficiency, between the images acquired with 5 mm gating window (reference), with the images acquired using an adaptive gating window with a fixed gating efficiency of 25%, 50%, 75%, and 100%, are in bold.

| Method (n=11) | GW (mm) Mean \pm std | Scan efficiency (%) Mean \pm std | p -value (T-Test) (α %) vs. (5 mm) | p -value (F-Test) (α %) vs. (5 mm) |
|-----------------|---------------------------|---------------------------------------|---|---|
| GW= 5 mm | 5.0 \pm 0.0 | 57 \pm 9 | - | - |
| α = 25% | 2.0 \pm 0.9 | 35 \pm 4 | <0.01 | <0.02 |
| α = 50% | 4.3 \pm 2.2 | 55 \pm 3 | 0.42 | <0.01 |
| α = 75% | 8.1 \pm 3.1 | 77 \pm 4 | <0.01 | <0.03 |
| α = 100% | 15.3 \pm 6.4 | 97 \pm 1 | <0.01 | <0.01 |

Table 2

Mean \pm standard deviation (std) of the segmented subjective score and the overall normalized vessel sharpness of the targeted right coronary artery (RCA) images acquired from 11 subjects using a diaphragmatic navigator with 5 mm gating window (GW), and adaptive gating window with a fixed gating efficiency of 25%, 50%, 75%, and 100%, respectively. The subjective score is based on a four point scale (1-poor; 4-excellent). The quantitative vessel sharpness is a measure between 0 and 1. The statistically significant p -values comparing the images acquired with fixed 5 mm gating window (reference) with the images acquired using an adaptive gating window with a fixed gating efficiency of 25%, 50%, 75%, and 100% are in bold.

| Method (n=11) | Subjective score | | | Quantitative score | | |
|-----------------|------------------|---------------|---------------|--------------------|-----------------|-----------------|
| | Proximal | Middle | Distal | sharpness | p -value | p -value |
| GW= 5 mm | 2.4 \pm 0.8 | 3.0 \pm 1.0 | 2.0 \pm 0.8 | 0.57 \pm 0.08 | - | - |
| α = 25% | 2.9 \pm 0.8 | 3.4 \pm 0.7 | 2.4 \pm 0.9 | 0.60 \pm 0.07 | <0.05 | <0.02 |
| α = 50% | 2.4 \pm 0.9 | 2.9 \pm 1.0 | 1.7 \pm 0.8 | 0.56 \pm 0.10 | 0.28 | 0.74 |
| α = 75% | 2.2 \pm 0.9 | 2.4 \pm 0.8 | 1.4 \pm 0.5 | 0.56 \pm 0.09 | <0.01 | 0.65 |
| α = 100% | 1.5 \pm 0.9 | 2.2 \pm 0.9 | 1.1 \pm 0.3 | 0.52 \pm 0.11 | <0.01 | 0.12 |

\$watermark-text

\$watermark-text

\$watermark-text

Table 3

Mean \pm standard deviation (std) of the gating window size, the scan efficiency, and the subjective score of late gadolinium enhancement (LGE) left atrium (LA), left ventricular (LV), and phase-sensitive inversion recovery (PSIR) images acquired using the proposed adaptive gating window technique. The subjective score is based on a four point scale (1-poor; 4-excellent). All statistically significant p -values, comparing the actual scan efficiency using the proposed adaptive gating window and the projected scan efficiency using the fixed 5 mm gating window, are displayed in bold.

| Imaging sequence | α (%) | GW (mm) Mean \pm std | Scan efficiency (%) Mean \pm std | p -value | Subjective score Mean \pm std |
|-------------------|--------------|---------------------------|---------------------------------------|-----------------|------------------------------------|
| LGE LA (n = 29) | - | 5.0 | projected (38 \pm 21) | <0.01 | - |
| | 40-50 | 6.2 \pm 3.0 | actual (47 \pm 8) | | 3.4 \pm 0.7 |
| LGE LV (n = 19) | - | 5.0 | projected (47 \pm 14) | 0.68 | - |
| | 40-50 | 6.0 \pm 3.1 | actual (48 \pm 8) | | 2.7 \pm 0.9 |
| LGE LV PSIR (n=8) | - | 5.0 | projected (37 \pm 13) | 0.14 | - |
| | 40-50 | 6.3 \pm 3.0 | actual (48 \pm 7) | | 3.1 \pm 0.8 |